THREE DIMENSIONAL PROCESSING OF SILICON WITH PULSED LASERS FOR OPTICAL APPLICATIONS

A THESIS SUBMITTED TO

THE GRADUATE SCHOOL OF ENGINEERING AND SCIENCE

OF BILKENT UNIVERSITY

IN PARTIAL FULFILLMENT OF THE REQUIREMENTS FOR

THE DEGREE OF

MASTER OF SCIENCE

IN

ELECTRICAL AND ELECTRONICS ENGINEERING

By
Ahmet Turnalı
May, 2015

Three Dimensional Processing of Silicon with Pulsed Lasers for Optical
Applications
By Ahmet Turnalı
May, 2015

We certify that we have read this thesis and that in our opinion it is fully adequate,
in scope and in quality, as a thesis for the degree of Master of Science.

————————————————————
Assoc. Prof. Dr. Fatih Ömer Ilday(Advisor)

————————————————————
Prof. Dr. Orhan Aytür

————————————————————
Assoc. Prof. Dr. Alpan Bek

Approved for the Graduate School of Engineering and Science:

————————————————————
Prof. Dr. Levent Onural
Director of the Graduate School

ABSTRACT

THREE DIMENSIONAL PROCESSING OF SILICON WITH PULSED LASERS FOR OPTICAL APPLICATIONS

Ahmet Turnalı

M.S. in Electrical and Electronics Engineering

Advisor: Assoc. Prof. Dr. Fatih Ömer Ilday

May, 2015

Micromachining of silicon with lasers is being investigated for the last three decades. Until now, interior silicon modification without inscribing the surface has not resulted in success. Such an ability could enable disruptive technologies in nanophotonics by paving the way for producing monolithic optoelectronic chips. Here, we report a maskless, one step photo-induced method to generate subsurface modifications in silicon with pulsed infrared lasers for indefinitely large areas. We demonstrate continuous, highly controllable structures buried in the bulk of silicon wafers and investigate the underlying mechanism. Further, we utilize the method for spatial information encoding and fabrication of optical components in the infrared regime in silicon. This silicon processing technology can be useful in various applications, including multilayer silicon chips, solar cells and optofluidics.

Keywords: Silicon, Subsurface, Three dimensional, Laser, Processing.

ÖZET

OPTİK UYGULAMALAR İÇİN SİLİKONUN ÜÇ BOYUTLU İŞLENMESİ

Ahmet Turnalı
Elektrik-Elektonik Mühendisliği, Yüksek Lisans
Tez Danışmanı: Doç. Dr. Fatih Ömer Ilday
Mayıs, 2015

Lazerlerle silikon işleme uzun yıllar üzerinde çok sayıda çalışma yapılan bir konu oldu. Şimdiye kadar silikonun yüzeyine zarar vermeden, yüzey altı yapılar oluşturma çalışmaları başarıyla sonuçlanmadı. Böyle bir kabiliyetin olması, elektronik ve fotonik elemanların aynı optoelektronik çipin üzerinde birleşmesine elvererek yeni nesil mikroişlemcilerin yolunu açabilir. Bu çalışmada, silikonun yüzey altında yapısal değişiklik oluşturmak için kullanılabilecek maskesiz, ışıkla tetiklenen bir yöntem sunuyoruz. Atımlı kızıl-ötesi lazerlerin kullanıldığı bu yöntemle sadece kesiksiz, kontrol edilebilirliği yüksek yüzey-altı yapılar yapmakla kalmayıp, bu yapılarla iki optik uygulama gerçekleştirdik. Silikonun içine bilgi kodlayarak, onu bir optik depolama ortamı olarak kullanmak ve kızıl-ötesi bölgede çalışan optik bileşen inşa etmek, ortaya çıkardığımız uygulamalardan. Bu özgün silikon işleme teknolojisinin silikon yongaları, güneş pillerini de içeren çok sayıda alanda faydalı olacağını düşünüyoruz.

Anahtar sözcükler: Silikon, yüzey altı, üç boyutlu, lazer, işleme.

Acknowledgement

I would like to thank my supervisor F. Ömer Ilday for his continuous support, guidance and patience during my studies. I am very grateful to have the opportunity to work with him. I am also indebted to Onur Tokel and Ihor Pavlov for fruitful discussions and for their support in various stages during experiments.

I would like to express my gratitude to Tahir Colakoglu from METU for his efforts in chemical etching of silicon and providing SEM images. I also would like to thank Serhat Tozburun, İmran Akça from Harvard University for taking OCT images of embedded barcodes inside silicon.

I thank my committee members, F. Ömer Ilday, Orhan Aytür and Alpan Bek, for sparing their time in their busy schedules and accepting to be on my committee and also for their helpful feedback.

I am also grateful to all members of Ultrafast Optics & Lasers Group for making the thesis procedure fun.

Contents

List of Figures

List of Tables

Chapter 1

Introduction

1.1 Motivation, Objectives and Review

Integrating photonic elements with conventional integrated circuits is a crucial step for designing new generation microchips [1, 2]. To accomplish this, one needs to be able to fabricate optical elements that can create, manipulate and detect light on the same chip with electronic circuits [3]. So far, studies have been focused on manufacturing those elements only on the surface of silicon. This is due to the limitations of current fabrication methods. Etching and lithography, two of the most common micro-fabrication techniques in CMOS technology, modify the substrate layer by layer which prevents the formation of components along the vertical axis. Therefore, they can exploit only the top thin layer of the surface.

Using direct-laser writing methods on silicon, various patterns that result different functionalities have been demonstrated. Microcolumn arrays and surface ripples were created by using laser diffraction on the surface of silicon [4, 5]. Black-silicon, which increases absorption of light in infrared range, is the result of treatment of silicon with laser. Such advances are highly desirable in solar cell or thermal imaging applications [6, 7]. Moreover, silicon surface properties can be modified with laser-writing. Silicon can be transformed to superwicking

when the surface is treated with pulsed laser [8]. All these works modified the optical and physical properties of silicon in a controlled manner, and are good examples of the capabilities provided by laser-silicon interaction. However, these photo-induced effects take place on the surface. Until now, a controlled method that can create such effects in subsurface silicon has not been discovered.

The only way to introduce these elements and functionalities into the bulk of a material is by processing in the transparent regime. For three-dimensional structures, extensive studies have been conducted, especially in glass and polymers [9, 10]. Since linear absorption is small for transparent materials, only non-linear processes such as multi-photon absorption or avalanche ionization can create those effects [11, 12]. In order to induce such effects, high intensities are necessary, and can be achieved with focused pulsed lasers. When a laser beam is focused into a material, a refractive index change is generated and the refractive index difference between processed and unprocessed areas can be utilized for creating optical elements.

Using this approach various optical elements have been fabricated in the bulk of silica and crystals such as lithium niobate or bismuth germanate. Those elements include waveguides, interconnects and resonators [13, 14, 15]. Moreover, structures created with that mechanism can be also used as a part of a more complicated photonic device. For instance, they can be used to create phase difference in the optical paths of 3D Mach-Zender interferometer in a microfluidic chip [16], or can be used in digital gate design for qubits in quantum optical circuits [17, 18]. Although, all these applications are examples of three-dimensional structuring of transparent materials, these devices are not CMOS compatible and capability to integrate them with the conventional electronic chips is very limited.

Silicon, on the other hand, is the backbone of CMOS technology. It has always been a great interest to extend the planar topologies to three-dimension in silicon [19]. That development can lead cost-effective and high-efficiency integration of optical elements into electronic chips [20]. This thesis introduces a method to inscribe fully continuous, highly controllable, photo-induced subsurface modifications buried in silicon without any surface damage. With this technique, it

is possible to fabricate structures in indefinitely large areas with various geometries. Similar to laser written structures in silica, modifications in silicon are the result of nonlinear interaction of laser with the substrate. This fabrication technology can benefit multiple fields, including silicon photonics and optofluidics. Moreover, by adding a new dimension, it may improve chip capacities drastically. Since it is an optical process, instead of a chemical one, the introduced method adds a new capability to current silicon fabrication literature. The thesis also introduces novel ways to image inside the silicon, which can be used to characterize the structures precisely. As a demonstration of the capabilities obtained with this method, two optical devices, Fresnel zone plate and three-dimensional silicon memory, are created and characterized.

1.2   Organization of the Thesis

The rest of the thesis has the following structure. General overview of the laser-transparent material interaction is given in Chapter 2. This is to give an overview of possible mechanisms of subsurface silicon inscription. In Chapter 3, experimental setups that we constructed for the experiments are described in detail. Chapter 4 explains the imaging methods we developed for characterizing the structures. Mechanism and results of the optimization studies are presented in Chapter 5. Also, in that chapter, details of the designs and the characterizations of the applications are explained. In the last chapter, concluding remarks are given.

Chapter 2

Laser-Matter Interaction in the Bulk of a Transparent Material

Laser-matter interaction in the bulk of a transparent material is different than the interaction on the surface, since in the former, the interaction is confined inside a closed space within the solid. High energy density in such a small volume, depending on the damage threshold of the material, can change the optical and structural properties in the exposed region. Such changes can be manipulated to fabricate optical devices like waveguides, photonic crystals or memory bits.

In the low power density regime, only phase transition may be induced by laser. When applied power is above ionization threshold, material at the focal point is transformed into hot plasma. Depending on the amount of exceeding power, final structure of the processed area may vary. In case of further heating of the material, shockwave formation and low density regions, i.e, voids, may occur within the focal volume.

2.1 Laser-Material Interaction Overview

Electronic bandgap of a material determines the wavelengths in which the material is transparent. If the energy of the photon is smaller than the bandgap, it can not excite any electrons to higher energies resulting in transparency. To modify the material at such wavelengths, nonlinear effects must be induced in the material, which is only possible at high intensities. Another important feature of the dielectrics is thermal conductivity. In general, thermal diffusion constant is two order of magnitude lower than the metals. In other words, heat will take more time to dissipate in the exposed region. Therefore, even though a single pulse may not be sufficient to induce any changes in the material, high repetition rates can exploit this accumulation effect and modification can be produced.

When a laser beam is focused inside the material, electrons start to oscillate. With the random collision of electrons with atoms, electrons gain energy from the oscillating field and electron excitation occurs. After that, this energy is transferred to the lattice either by electron-phonon collisions or electron heat conductions. Depending on the heat transfer type, equilibrium of energy is finalized over a period proportional to temperature equilibration time (t_{e-L}) or heat conduction time (t_h). Relations of these energy distribution times with pulse duration determine whether the absorption occurs at the end of the pulse or during the energy deposition. Difference between these two cases effects the critical absorption parameters such as absorbed energy and maximum temperature in the focal spot. In general, absorbed energy in the laser propagation direction can be obtained as follows [21]

$$Q = \frac{w}{c} \frac{4\epsilon}{(1+\sqrt{\epsilon})^2} I(r,z,t) \equiv \frac{2A}{I_{abs}} I(r,z,t) \tag{2.1}$$

where A is the absorption coefficient in Fresnel equations and l_{abs} is the electric field absorption depth. I(r,z,t) is the intensity of the beam. A and l_{abs} are defined as:

$$l_{abs} = \frac{c}{w\kappa} \quad , \quad A = 1 - R = \frac{4n}{(n+1)^2 + \kappa^2} \tag{2.2}$$

Here, n and κ are the real and imaginary parts of the complex refractive index, respectively. Maximum energy is absorbed at the beam waist (z = 0, r = 0). Due to small interaction volume and the high energy absorption at the beam waist, temperature rise at the waist is maximum on the laser propagation axis. In such a condition, maximum temperature can be calculated with the following:

$$T_{max} = \frac{2AE_{pulse}}{Cn_a} \frac{1}{\pi r_0^2 I_{abs}} \tag{2.3}$$

where, C and n_a are specific heat capacity and atomic density of the lattice. Laser energy per pulse and beam radius in the focal spot are represented with E_{pulse} and r_0. Volume of the modifications depends on the maximum achievable temperature directly. If temperature is within the range of non-destructive phase transition, modified area will have a diameter around the beam size. On the other hand, when plasma is induced in high-intensity regime, interaction mode changes and interaction volume becomes smaller than the focal volume due to high absorption of plasma.

Effect of the temperature on material modification can be visualized by assuming incremental change of laser power from low power regime to high power regime. First, with the increase in the intensity the optical properties of the material changes. When temperature hits a critical spot, phase transitions occur. This phase transition can be as a result of melting and rapid resolidification or just amorphization without any change in the state of material. Until this point, dominating mechanism is inter-band transitions where single or multi-photon absorption plays an important role. This regime can also be called low-intensity mode. Further increase in the temperature results in material decomposition by ionization, detachment of the atomic bonds. For such modifications, high-intensities are required. Any further increase in the intensity doesn't change the mechanism fundamentally, but physical properties of the modification can be effected by the temperature of the created plasma [9].

2.2 Governing Mechanisms at High Intensity

High intensity laser-material interaction occurs when the electron oscillation energy in the laser generated electric field is approximate to the band-gap energy. In this case, laser-material interaction is different than low intensity regime. Generated plasma increases the absorption of the incident light and creates a high energy density at focal point, which results in high refractive index change. Thus, a controllable modification for photonic applications is possible with that process.

Plasma is formed as a final product of material ionization. Depending on laser parameters such as pulse duration, intensity, wavelength as well as material properties, either impact (avalanche) ionization or multi-photon ionization can be dominant mechanism for material modification. In avalanche ionization, excitation of electrons in the valence band by direct absorption is negligible. Available electrons in the conduction band gain energy by collisions during the oscillations in the laser generated electric field. When those excited electrons (seed electrons) have energy higher than the bandgap ($\varepsilon > \Delta_{gap}$), they can excite the valence band electrons to conduction band by collision. The probability of exciting electrons with impact ionization (w_{imp}) is directly proportional to the laser intensity and given by:

$$w_{imp} \approx 2 \frac{\varepsilon_{osc}}{\Delta_{gap}} \frac{w^2 v_{eff}}{v_{eff}^2 + w^2} \tag{2.4}$$

Here, ε_{osc} is the electron oscillation energy, w is the laser frequency and v_{eff} is the effective collision rate of electrons. This equation also shows that probability increases with the square of the laser wavelength. However, electron-lattice collision rate v_{eff} saturates at the plasma frequency after a certain temperature level. At these levels, $w < v_{eff}$ holds and frequency dependence of the probability diminishes [22]. However, for both probability equation and such assumptions to be correct, classical approach must be valid. A dimensionless parameter γ can be checked for this purpose.

$$\gamma \approx \frac{\Delta\varepsilon}{\hbar w}\frac{\varepsilon}{\hbar w} \qquad\qquad (2.5)$$

In case of $\gamma > 1$, classical treatment can be applied for calculation of avalanche ionization probability. This means that for classical approach, both the electron oscillation in one collision and electron energy must be greater than the photon energy.

Optical breakdown occurs when excited electron density (n_e) reaches a critical level (n_c), i.e., $n_e = n_c$. Therefore, it should be noted that even though w_{imp} is high, that doesn't guarantee avalanche ionization. Initial electron density (n_0) must be high enough that during pulse duration, excited electron density can reach critical density of electron for breakdown threshold at a specific laser frequency. Generated electron density by avalanche process and critical electron density are given as:

$$n_e(t) = n_0 2^{w_{imp}t} \qquad , \qquad n_c = \frac{m_e w^2}{4\pi e^2} \qquad\qquad (2.6)$$

Other important mechanism in the high-intensity regime is multiphoton ionization. The mechanism can start at relatively low intensities and there is no threshold for it to start. It only depends on absorption of several photons at the same time. Seed electrons created by this process can grow by the avalanche process. Whether tunneling ionization or multi-quantum photo-effect will be effective during the multiphoton absorption can be determined by checking the Keldysh parameter. It is defined as the ratio of electron oscillation energy to bandgap energy and when $\varepsilon_{osc} >> \Delta_{gap}$ holds tunneling ionization is dominant process. However, in both cases the probability of multiphoton ionization doesn't change and can be calculated as:

$$w_{mpi} \approx w n_{ph}{}^{3/2}(\frac{\varepsilon_{osc}}{2\Delta_{gap}})^{n_{ph}} \qquad where \qquad n_{ph} = \frac{\Delta_{gap}}{\hbar w} \qquad\qquad (2.7)$$

One limitation of high-power interaction regime is that in the presence of excessive optical power, focusing the incident beam to a desired point may be

prevented by some non-linear effects. Intensity-dependent part of the refractive index increases as the power rises. Therefore, due to nature of the Gaussian beam, refractive index on the optical axis becomes higher than the rest of the interacted area. As a result, self-focusing effect occurs. The critical power for self-focusing can be calculated as [23]

$$P_{cr} = \frac{\lambda^2}{2\pi n_0 n_2} \tag{2.8}$$

After creation of plasma with self-focusing, plasma deflects the rest of the beam. However, if the incident light has power several times higher than the that threshold, deflected light can also go through self-focusing and instead of a point modification in the focal area, filaments can be obtained in the optical axis. For that, generally, laser power must be $> 3P_{cr}$ [24].

2.3   Optical Properties of Silicon

If a material is going to be used as a medium for three-dimensional structuring, certain properties of that material should be studied. This is necessary for both laser source selection and nonlinear response estimation. Therefore, linear and nonlinear part of the refractive index as well as transmission spectra of the material must be known. Using these information, specifications of experimental setup can be deduced and by comparing the results with calculations, underlying mechanism can be revealed. Optical property studies for silicon indicates that absorption coefficient is near zero for the spectral range between 1.2 μm to 7 μm [25]. Moreover, linear refractive index, $n_0 = 3.47$ and nonlinear refractive index, $n_2 = 4.10$ $^{-14}cm^2/W$ at our operation wavelength (1.55 μm)[26].

Chapter 3

Experimental Setup

The method we developed for interior silicon structuring is rapid and very promising for multiple applications, including photonic crystals, waveguides or optical data storage. The technique is a maskless, single step photo-induced process and doesn't require any chemical treatment. For modifying subsurface silicon, we employ a high-power fiber laser system working at 1.55 μm, producing nanosecond pulses. Laser output collimated from this system is directed to processing station. Here, laser parameters are adjusted and laser beam is tightly focused inside silicon such that conditions are sufficient to stimulate nonlinear processes like multiphoton absorption without causing any surface modification. During experiments we found that to create modification in the bulk of silicon, controlling the beam characteristics is not enough by itself. Precise sample alignment and sample properties are also very critical elements in determining location and morphology of the structures. Therefore, laser setup, processing station and sample selection the three main categories which we will explain in detail.

3.1 Laser System

As stated in Chapter 2, to process bulk of a material, laser wavelength should be in the range where the material is transparent. Therefore, for subsurface processing of silicon, it is apparent that a laser with 1.2 μm or longer wavelengths are suitable for our purposes. However, satisfying this condition isn't adequate on its own for interior writing of silicon. Typical threshold intensities for subsurface laser writing in a dielectric is around 10^{14} W/cm^2 [27]. Therefore, the laser system must supply enough power such that with efficient focusing, it can reach this intensity levels at the focal spot. Moreover, a pulsed laser must be used instead of continuous wave laser, since threshold intensity can not be reached with CW lasers.

Considering these specifications, we decided to utilize a home-built all-fiber-integrated master oscillator power amplifier (MOPA) system that works at 1.55 μm and produces 5.5 ns, 5 W pulses with 150 kHz repetition rate [28]. The schematic of this system is shown in Figure 3.1.
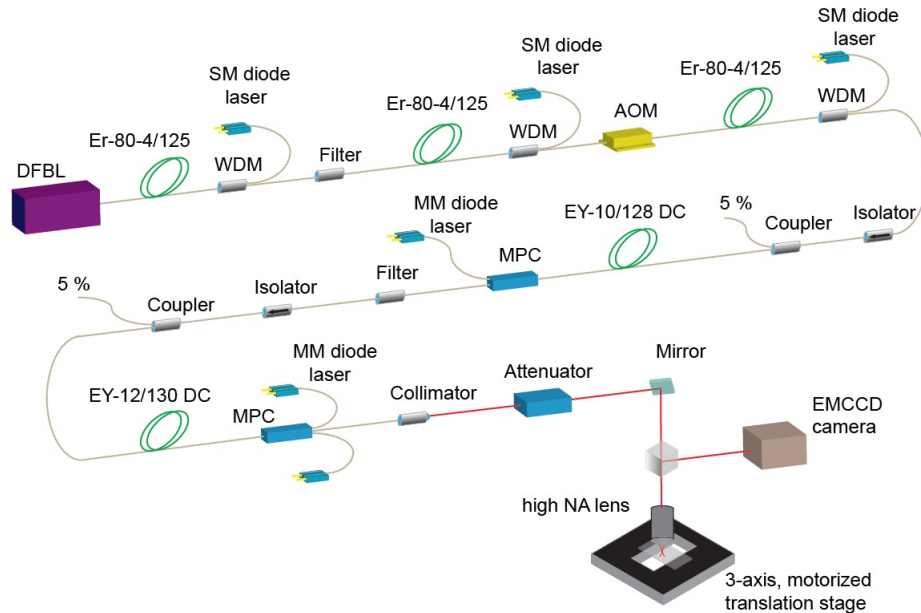
Figure 3.1: Schematic of laser setup.

The system obtains the seed pulses, signals that are going to be amplified, by modulating a low-power, single-frequency distributed feedback semiconductor

laser (DFBL). Current modulation of DFBL allows control over the pulse duration of seeds and the shortest duration achievable with this method is 10 ns. Limitation in the maximum amount of current that DFBL can handle sets an upper bound for the pulse energy. With the shortest duration and maximum current, this limit is about 1.5 nJ. In order to get the maximum signal power possible and saturate the following pre-amplifier, modulation frequency is adjusted to 150 kHz. Temporal profile and the optical spectra of the seed signal can be seen in Figure 3.2.
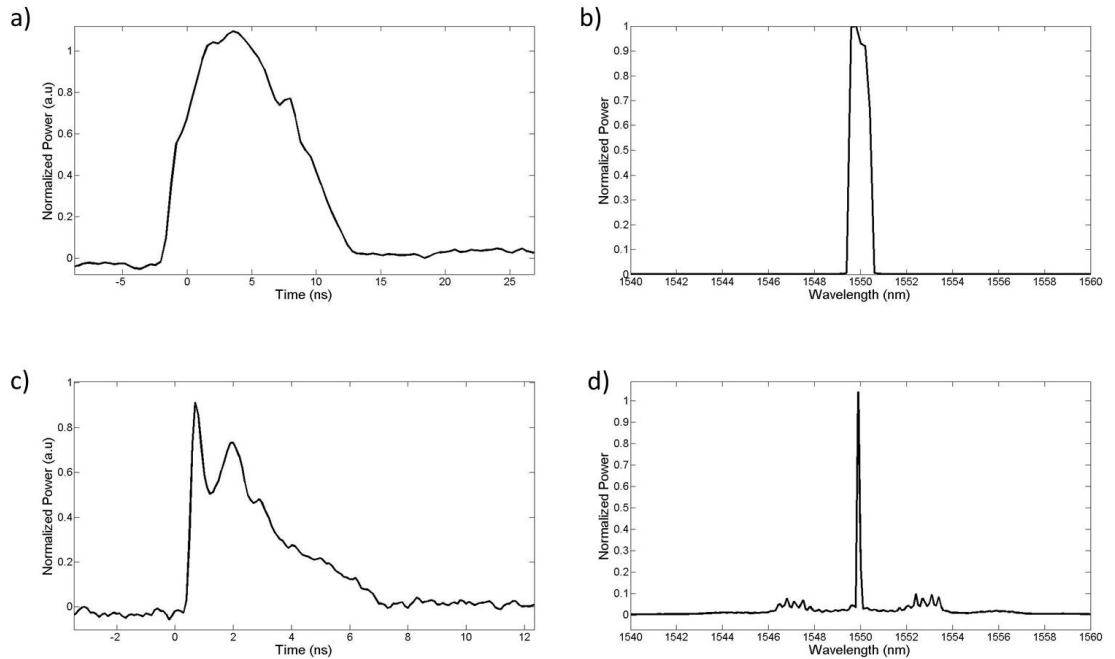
Figure 3.2: (a) Temporal profile of seed signal. Pulse duration is approximately 10 ns. (b) Output spectrum of seed signal. (c) Temporal profile of amplified signal. $\tau \approx 5.5$ ns. (d) Output spectrum of amplified signal.

The seed signal goes into two pre-amplifers, which are Er-doped fibers pumped by a single diode operating at 976 nm and it is amplified to 120 mW. Acousto-optic modulator (AOM) at the output of the preamplifiers is used to suppress ASE in time domain by blocking accumulated ASE between pulses and by allowing only the pulses to the next stage. Utilizing narrowband bandpass filters between the amplifier stages also eliminates ASE due to broadband nature of ASE. The first amplifier stage after AOM is Er-doped and pumped by a single mode diode at 976 nm. As a result, seed pulse is amplified to 169 mW.

The last two stages consist of Er-Yb codoped gain fibers. The reason for using codoping is to increase output power. Since Er-doped fibers have lower pump absorption than Yb-doped fibers, it isn't possible for Er-doped fiber lasers to reach peak-power levels that are achievable with Yb-doped ones. To address this problem Yb-ions are implanted with Er-ions. Although, this technique introduces high ASE generation problem, it is possible to overcome this issue with the usage of AOM and bandpass filter as explained. In our system, that method allows us to have 10W of average power, which corresponds to the highest pulse energy for 1.55 μm with current configuration. At the end of the last amplifier stage, standard single-mode fiber is used to get the system output. Temporal and spectral profile of the pulses that we use in our experiments can be seen in Figure 3.2.

3.2   Processing Station

To be able to cover a wide set of experiments, processing station must be designed carefully. It must allow changes in laser parameters such as power and polarization. Beside that, it must provide high precision laser movement on sample in a controllable manner. Further, it must be robust so that experiments can be reproduced with good confidence and reproducibility. Schematic of our setup is shown in Figure 3.3. This system has three main parts: Power attenuator, monitoring system and translation stage. The first part is designed to manipulate laser parameters such that effect of those parameters on mechanism can be investigated. Monitoring system is both for alignment of the samples and also for in-situ imaging of the process. Lastly, we use translation stage to locate beam to desired position in silicon.

Fast control over laser properties without redesigning the laser configuration is critical. This provides a parameter set available for experimenting by using a single laser setup. For this purpose, we built a power attenuator with polarization control ability. It consists of two polarizing beam splitters (PBS) and a half-wave plate (HWP) between them. Beam splitters in our system reflects vertical polarization (s-polarization) by 90^0. By rotating the polarization plane with the help
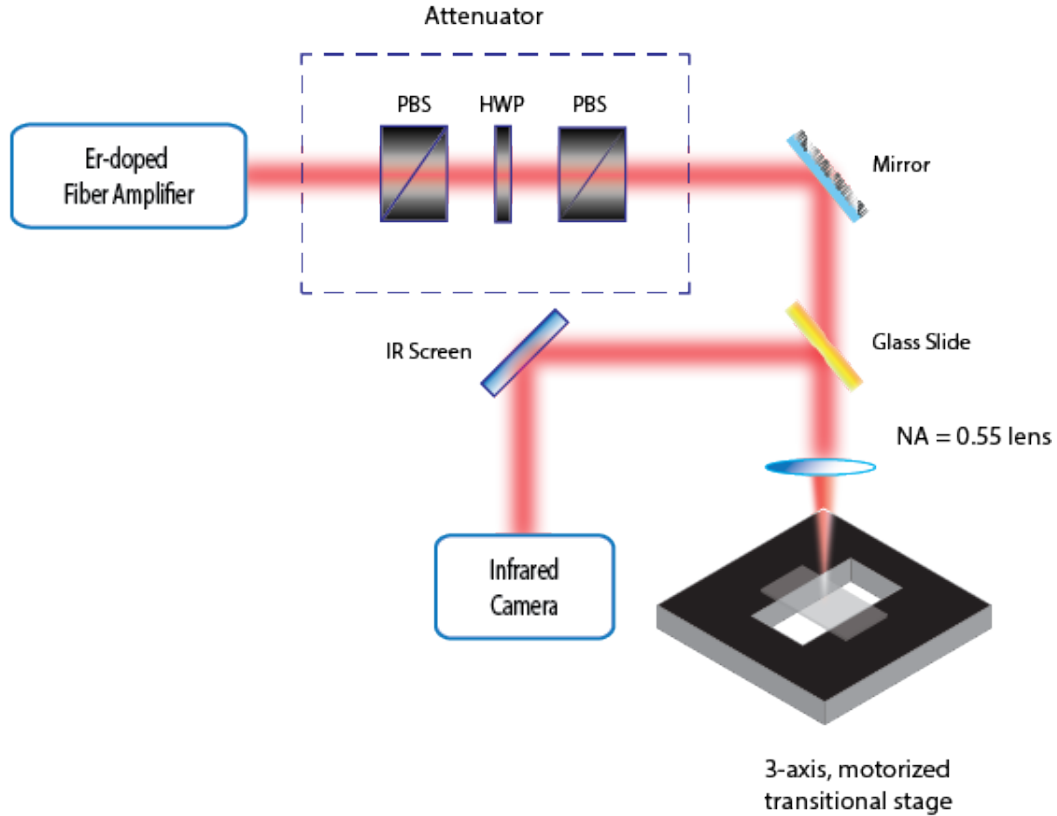
Figure 3.3: Processing station schematic for silicon inscribing. PBS: polarizing beam splitter, HWP: half wave plate, NA: numerical aperture.

of HWP, we can control the percentage of the transmitted light through 2nd PBS. With this configuration, we can scan a power range from almost 0% to 77% of total power received from MOPA. Upper limit for transmission has been set by the total insertion loss of the components in power attenuator. After attenuator, laser always has horizontal polarization. A wave retarder is placed after attenuator to set the final polarization. Another advantage of this system is that it is possible to enhance its capabilities by adding new experimental parameters to current parameter set. An example of this would be repetition rate or number of pulses, which can be designed by inserting a chopper wheel or a shutter into the system.

One of the superior features of our method is that we can process silicon for indefinitely large-areas. It is only limited by the capacity of the translation stage holding the sample. A critical condition for utilizing this restricted scanning
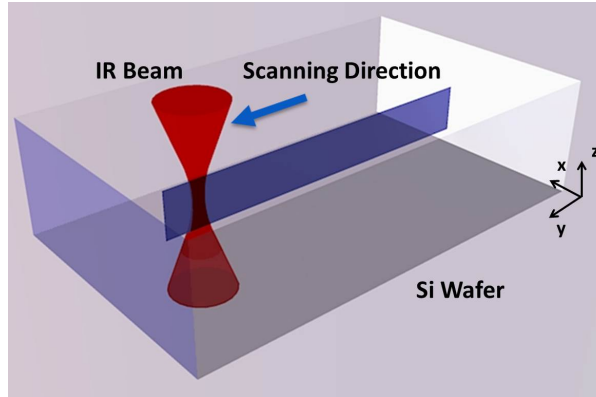
Figure 3.4: Tightly focused laser beam creating the high-aspect ratio structures within the wafer.

area with maximum efficiency is maintaining the same operating state. This is achievable with precise sample alignment. In perfect alignment, incident laser beam is perpendicular to silicon sample throughout the scanning range. To ensure that, we exploit back reflections from the silicon. Reflected light from both front and back surfaces of the sample are directed to an infra-red sensitive camera by using a glass slide. By minimizing interference spot in low-power mode, we place the waist of the beam on front surface of silicon. Radius of the first bright fringe changes during scanning if surfaces are misaligned, i.e., there is an angle between the laser propagation direction and the surface normal. The monitoring system is also utilized for *in-situ* imaging of inscribing, which is quite useful for rapid analysis of structure quality.

We mount the sample to a 3-axis, motorized stage. This programmable stage makes the processing automated. Therefore, otherwise time-consuming structures and modifications with different complexities, from lines to curved structures such as concentric circles, can be inscribed with relative ease. In Figure 3.4, an illustration of silicon inscription is presented by a linear motion in one axis using the stage.

3.3   Sample Selection and Preparation

For our experiments, double-side-polished, <100>, 500 μm thick, p-type (Boron-doped 6Ω.cm), n-type (Phosphorus-doped 1Ω.cm) and undoped (15 kΩ.cm) wafers were used. These set of sample parameters, except doping level, are finalized as the result of experimental optimization, which is one of the subject of this subchapter. As explained in previous section, back reflections from both surfaces are utilized for locating the beam focus on the front surface of silicon. Therefore, we used double side polished wafers. With one-side-polished wafers, this operation can't be accomplished and alignment within the scanning range can't be done with micrometer level precision, which are both important requirements for high quality structures. Although, in principle, any silicon thickness is acceptable for processing, thickness of the samples must be suitable for proof of concept experiments, such as optical memory which requires writing multilevel-structures. In commercial wafers with less than 500 μm thickness, only one layer of modification can fit without damaging the surface. Upper limit for silicon thickness is set by maximum power that laser system can supply. If necessary power to process deeper parts of the silicon is higher than maximum laser power, rest of the sample after that level will remain unused. Thus, 500 μm seems to be optimal value as sample thickness. Using different doping type and concentrations helps to understand the mechanism better in terms of the role of light-electron interaction. Detailed analysis and the results showing the effect of the doping is given in Chapter 5.2.2.

Another optimization for our experiments is done on sample sizes. The criteria in determining the size of the samples is maximizing the number of structures on the wafer as well as making precise alignment possible. Although all samples are taken from the same type of wafers, many properties that can effect the experiments, such as doping concentration, thickness etc. may vary slightly for different wafers. To minimize the undesired outcomes originated from that issue, machining the same sample as many times as possible is desired. This means that silicon piece must be moved on sample holder such that laser can be placed on every point on the sample. Due to restriction imposed by sample holder size, this

requires making the silicon sample as small as possible. While doing that, the minimum sample sizes required for high quality alignment should be considered. As a result, experimentally, optimal dimensions that satisfy both high number of processing per sample and precise alignment conditions is found 1.5 cm x 3.2 cm.

During the experiments, we realized that both organic and inorganic residues on the surface can cause unexpected results. Organic residues can decrease the damage threshold of the surface, resulting in surface ablation. These modifications on the surface can either effect the continuity of subsurface structures or prevent formation of them totally. To mitigate this effect, organic residues are cleaned by immersing the samples in piranha solution on regular basis. Each time, we hold them in piranha for 10 minutes. To finalize the cleaning, samples are hold in acetone (5 minutes), ethanol (5 minutes), deionized water (5 minutes) and dried by using nitrogen. Inorganic residues can cause similar problems. Silicon dust from intentional surface modifications we induced for marking the surface of silicon can land various places on the sample. After a couple of experiments, accumulation of the dust is enough to be a possible problem for next trials. Therefore, before beginning each experiment, substrate must be cleaned in a way similar to previous procedure. For cleaning, we use acetone across the sample for 1 minute, followed by isopropanol for 1 minute and we dry them using nitrogen flow.

Chapter 4

Imaging of 3D interior volume of silicon

Since Si subsurface scribing is a novel, new technology, 3D imaging methods for interior are non-existant. Here, we developed four different methods to image the subsurface structures in silicon. These techniques have been used widely for other purposes in the literature and they are applied for imaging of interior volume of silicon for the first time in this study. We use infrared microscopy to assess overall quality of the modifications and measure their length in laser propagation direction. Scanning electron microscopy is beneficial for cross-section analysis and determining the effect of processing in perpendicular plane to laser propagation. Another method for cross-section studies is chemical etching. This method also gives information about the crystal structure in the processed area. The fourth technique for subsurface imaging is optical coherence tomography. Advantage of this method is that it can show 3D structure of the modifications, which contains complete information about physical properties. To ensure that the methods work properly, i.e, gives accurate, reproducible results, we used at least two of the methods together and we confirmed that they are consistent with each other. That means with these methods, we can obtain the physical characteristics of the structures, like length and width, to a very high certainty.

4.1 Infrared Microscopy Imaging

After laser-writing, the quality of the structures are studied with a home-made infrared microscope working in transmission mode. Schematic of the system is shown in Figure 4.1. A tungsten-halogen lamp is used as a near-infrared light source. Light coming from the source is collimated by a low NA lens and the transmitted light through the sample is collected with an objective. Depending on the purpose, magnification changes from X10 to X40. A sensitive EMCCD camera is used as detector. For high quality images, another low NA lens, as a collimator, and optical filter are placed between the camera and the objective. A computer controlled 2-axis translational stage is used as sample holder.
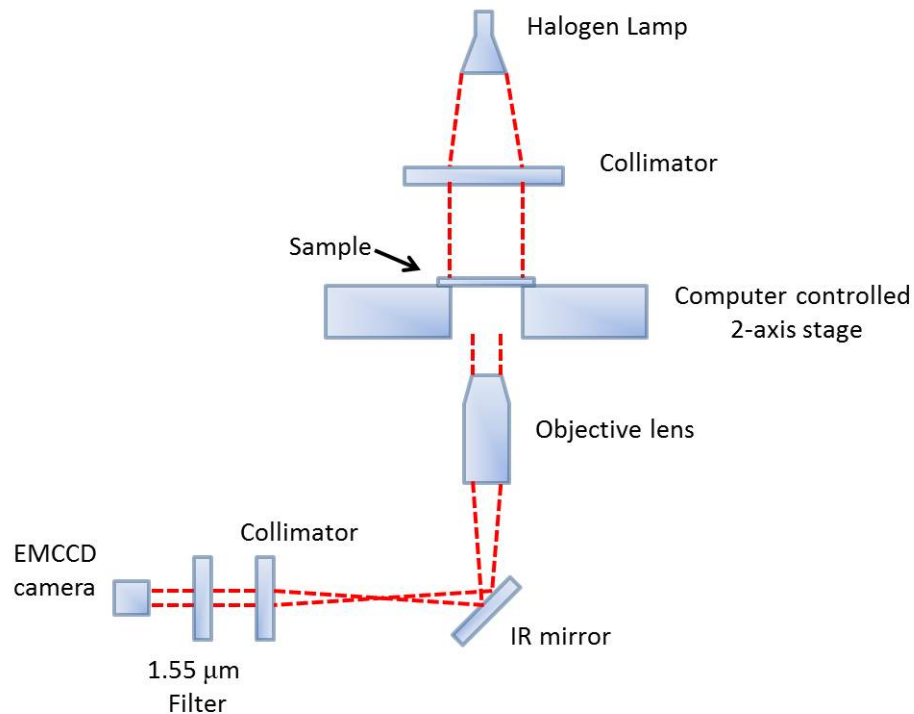
Figure 4.1: Representative schematic of IR microscope

This imaging system allows us to measure the length of high-aspect ratio (wall-like) structures as well as determine the quality of them,i.e, continuity, roughness and surface damage. For surface modification analysis, we also used a reflection mode microscope. By doing that, we can check the surface condition after the experiments to observe if there is any change induced by laser. For accurate length

measurement of the modifications, we measure the distance from surface to the point where structures start to emerge in silicon by moving the imaging plane of the microscope (d_{top}). We repeat the procedure but from the other surface and we find the distance between the bottom of the walls and back surface of silicon (d_{bottom}). Therefore, wall length, d_{wall}, can be calculated as $d_{wall} = d_{wafer}$ - (d_{top} + d_{bottom}), where d_{wafer} is the thickness of the wafer, obtained by SEM data. Microscope images of top surface of a processed area and interior structures written in the same plane are shown in Figure 4.2. With the method explained, we measured the length of the structures in Figure 4.2.b around 300 μm. It is also apparent that there is no surface modification above the structures.
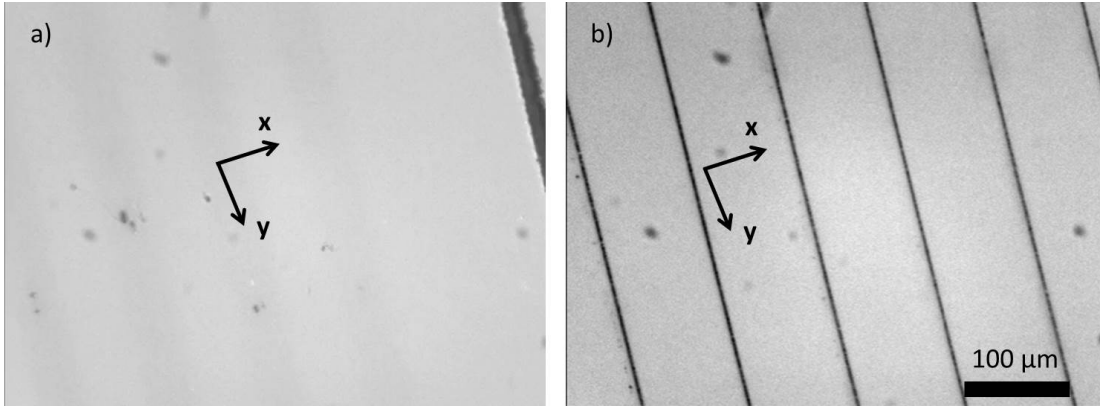
Figure 4.2: (a) Surface image of processed silicon. The line on the top right is intentional surface mark used as reference. (b) Microscope is focused underneath the surface. Lines seperated by 100 μm are visible.

4.2 Scanning Electron Microscopy

Scanning Electron Microscopy (SEM) was performed for the analysis of the cross-section of the structures. In addition to the width and length of the modifications, information regarding the mechanism can be deduced from SEM analysis. For convenience, only structures written with raster scan are studied with this method. In order to do that, we cut the wall-like structures into half in perpendicular to laser scanning direction using a dicer or a diamond cutter. A possible

problem with this technique is that, due to stress induced while cutting the sample for SEM, defect propagation can occur. This may cause observing longer structures than expected. Moreover, wavy structures can form due to the same reason and that may prevent measuring the real thickness of the structures.

In Figure 4.3.a, an SEM image corresponding to cross-section of the buried periodic structures can be seen. The structures seem to have a length of 350 μm. A close-up of a single line, given in Figure 4.3.b, indicates the width is approximately 1-2 μm. This shows SEM results has good agreement with the microscope results in terms of giving the width and length correctly. Further, detection of the modifications with SEM indicates that laser induces change in not only refractive index but also conductivity of silicon, since SEM is sensitive to conductivity of the material and the surface roughness remains the same for the modifications. This information can be used in explaining the mechanism of laser-material interaction.
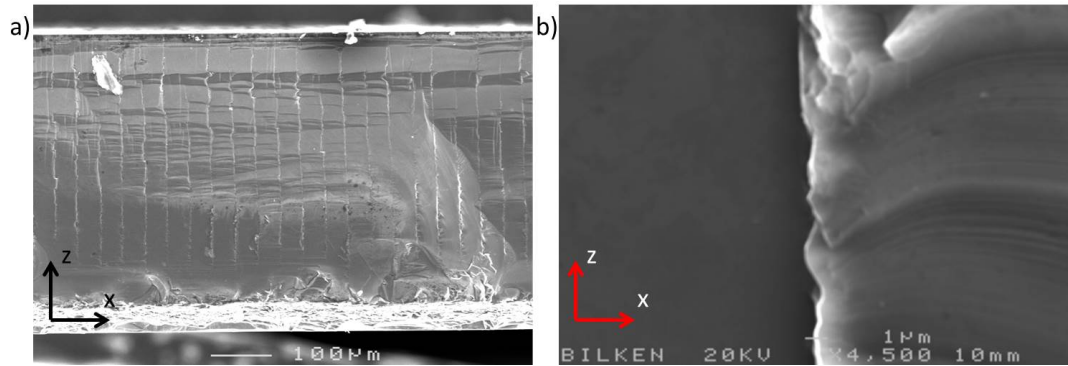
Figure 4.3: (a) General cross-section view of generated periodic structures. (b) Close-up of one of the structures. Thickness is approximately 1μm.

4.3 Chemical Etching

Conductivity change detected by SEM shows that during the laser process, phase transition from crystal to amorphous has taken place. Therefore, these structures can be manipulated with chemical methods which target only amorphous silicon and not interact with crystal silicon. Using such etchants reveal weakly processed

areas that aren't visible via microscope or SEM. For this purpose, we used several types of chemical compositions with different conditions. Empirically, we found that a solution called "MEMC etch" is the best option among other well-known defect characterization etchants for getting the sharpest etching of structures [29]. Figure 4.4.a shows the sample after treatment. Previously laser-modified areas are etched out, whereas the rest remains untouched. The width and length are 376 μm and 5 μm, respectively. These values are almost the same with SEM images of the corresponding modifications before etching, implying that all modified areas are visible with other methods. Moreover, etching the written structures can be used to create three-dimensional sculpturing similar to two-photon polymerization and etched structures can be utilized in microfluidic applications.
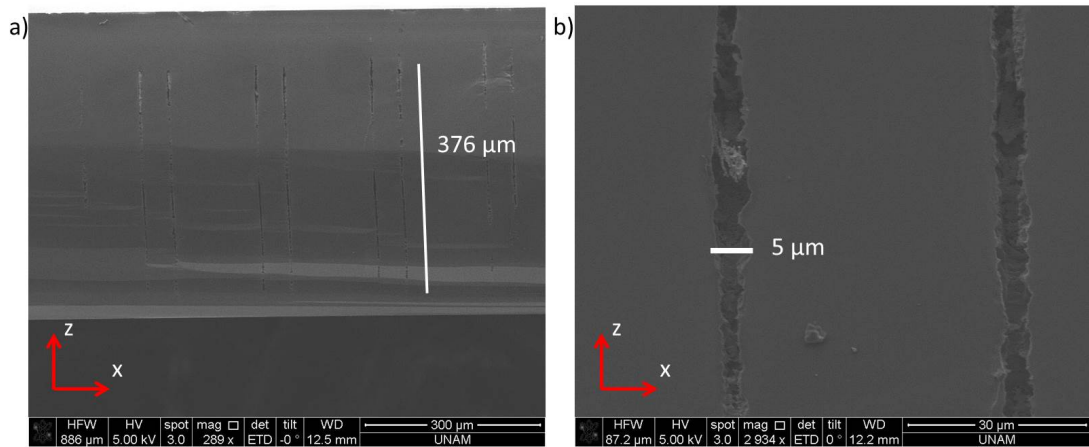
Figure 4.4: (a) SEM image of etched modifications. There are voids where modified areas were previously. (b) Zoomed in version the same sample. The depth of the crater can be increased with better optimization of the etchant.

4.4 Optical Coherence Tomography

Optical Coherence Tomography (OCT) is a well established imaging technique for biological applications [30]. It provides high-resolution, three-dimensional images within material by using scattering. However, to our knowledge, it has never been used for imaging of subsurface structures in any transparent material. Its

level by level reading capability is the perfect tool for retrieving written information from multilayer barcode system we designed. Since it is a non-invasive method, physical properties of the structures obtained with this system is free of any non-laser induced effect, like defect propagation. Moreover, using post-processing, refractive index of the modified silicon can be calculated. Figure 4.5 shows representative tomograms of subsurface modifications and readout of one barcode layer.

Figure 4.5: (a)-(b) Tomograms of structures obtained with different modalities. (c) OCT image of One layer barcode written in silicon.

The problem with OCT is that due to high refractive index of the silicon, strong back reflection can make the structures look longer than they are. However, this may be solved with post-processing the OCT data.

23

Chapter 5

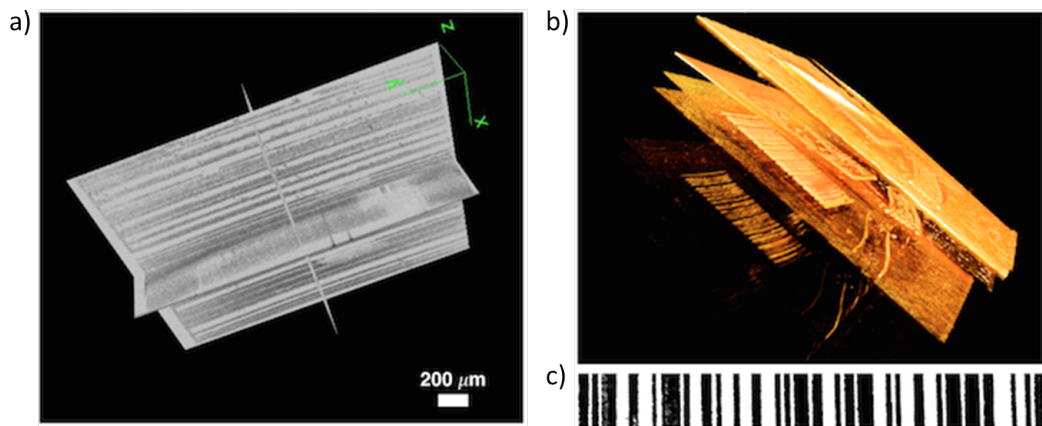# Physical Characterization, Mechanism and Applications

5.1 Physical Mechanism

To study probable physical origins of subsurface structures, we conducted a set of experiments. The first one is called raster scan, where laser beam is tightly focused with NA = 0.55 lens inside the silicon and 50 μm separated lines are inscribed on plane perpendicular to propagation direction with a scanning speed of 0.2 mm/sec. For each line, the laser scanning direction is alternated between two directions. This operation is done with a computer-controlled stage. We obtained continuous lines extending throughout scanning range, principally all the wafer but limited with stage's capabilities. This is exceptional, since such a range isn't easy to attain in various focused-laser methods for nano-patterning [31]. It shows that our method is quite promising as a future fabrication technique. Microscope image of a portion of processed area is shown in Figure 5.1.a.

When the cross section analysis of the modifications is studied by using SEM, as explained in Chapter 4.2, we observed that the length of the structure is over 350 μm, whereas Rayleigh length of the focused beam is 30 μm (Figure 5.1.b).

Considering the thickness of the modifications, which is approximately 1 μm, these periodic modifications deep in silicon has an aspect ratio over 200, making them to have a wall-like geometry. Occurrence of refractive index change further than the Rayleigh length and as a result of that, having another dimension in laser propagation direction is not observed in other transparent material writing experiments [32]. However, this striking feature is similar to filamentation effect in femtosecond laser transparent material processing [24]. As stated in Chapter 2, peak power of the pulse must be at least three times larger than P_{cr}, where P_{cr} stands for the critical power for Kerr-nonlinearity based self focusing. Using Equation 2.8, we calculated that $P_{cr} = 25.8 kW$ and peak power used for scribing the structures in Figure 5.1 is 4 kW. Although, comparison seems to be enough to prove that the mechanism is not filamentation, we believe an experimental proof is necessary.
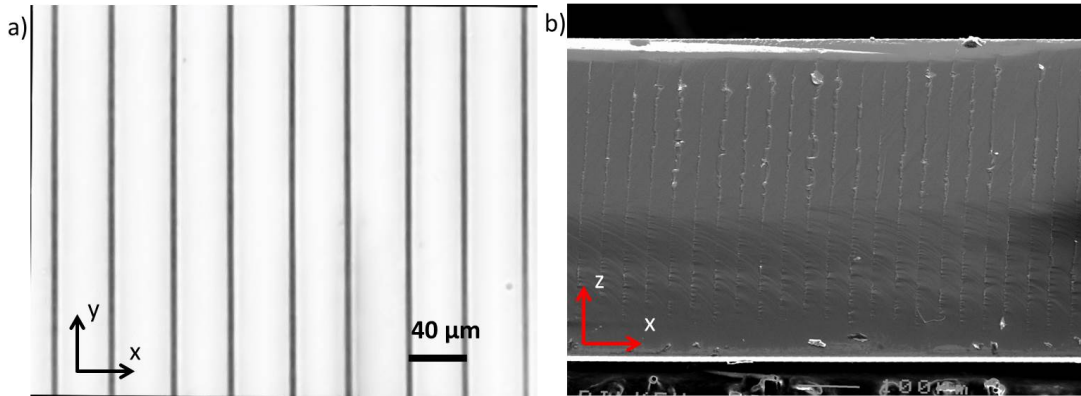
Figure 5.1: (a) Microscope image of subsurface silicon. Structures are in-focus, indicating they are underneath the surface (b) SEM image of the structures after the sample is cut into half perpendicular to laser scanning direction.

Experimental proof of filamentation is not the underlying mechanism is the existence of two different processing regime for silicon. In this experiment, we used a 1.3 mm thick, p-doped, double side polished (DSP) silicon wafer. We raster scanned the sample such that every other pair of the scanning was done on a plane deeper than the previous pair. For that purpose, after focusing the beam on the surface, we moved the sample 300 μm close to the lens and scribed the first pair of subsurface modifications. For the next pair, we moved the stage 10 μm closer. We repeated this procedure until the total movement of the sample is 470 μm. As

a direct result of Si-air interface, beam waist in silicon will be shifted from 1035 μm to 1620 μm [35]. Considering the thickness of the sample, when laser focus is moved 380 μm, focal point will be on the back surface. After that point, beam will be reflected and focused inside the silicon. All the laser parameters, such as polarization, pulse energy etc. as well as processing parameters like scanning speed are kept the same during the experiment. Figure 5.2 shows the result of this experiment. In the region where laser is focused directly into silicon, modifications are non-uniform and slightly discontinuous. However, when the laser is focused after reflection, the scribed lines are very thin and highly continuous. We tried combination of various parameters of energy and scanning speed to create similar structures in focus before reflection regime, however, thin and continuous modifications were not formed in any of them. If the filamentation was the main mechanism, it would be possible to obtain the same morphology before and after reflection regimes.
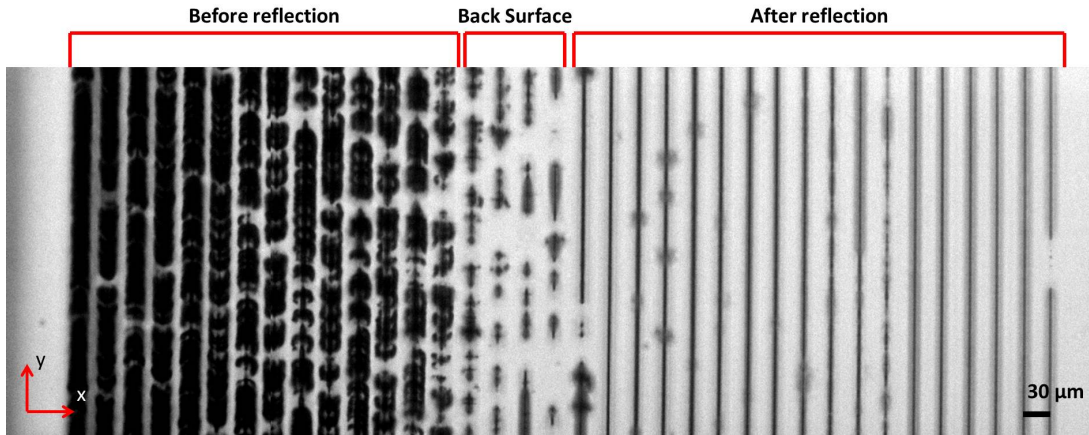
Figure 5.2: Microscope image of structures created at different depths. When incident beam is not reflected from the back surface, they form irregular structures. After reflection from the back surface, lines are thin and continuous. Image is taken when objective is focused at 400 μm depth.

The evident difference between modifications before and after reflection clearly indicates that back reflection plays a prominent role in creating high-quality sub-surface structures. In bulk processing of other transparent materials, like glass or polymers, such reflections are not taken into account [33, 34]. To test this hypothesis, we used pieces from an n-doped (1 Ω.cm) wafer that is double side polished (DSP), but on one side there are places coated with anti-reflective film,

which transforms those parts to single side polished (SSP). We raster scanned the sample in focus after reflection regime. Scanning started at DSP part, after some time laser beam enters SSP region. This enables us to process both DSP and SSP samples at the same time so that we can investigate the influence of back surface reflection. In DSP area, the structures were formed in a uniform and continuous manner. However, starting from the SSP-DSP boundary, laser writing is disrupted and modifications do not take place in anti-reflection coated area (Figure 5.3). This proves presence of strong reflection plays an prominent role in structure formation. Results of these two experiments are consistent with each other and both of them confirm that reflection is necessary to have wall-like structures with high uniformity.
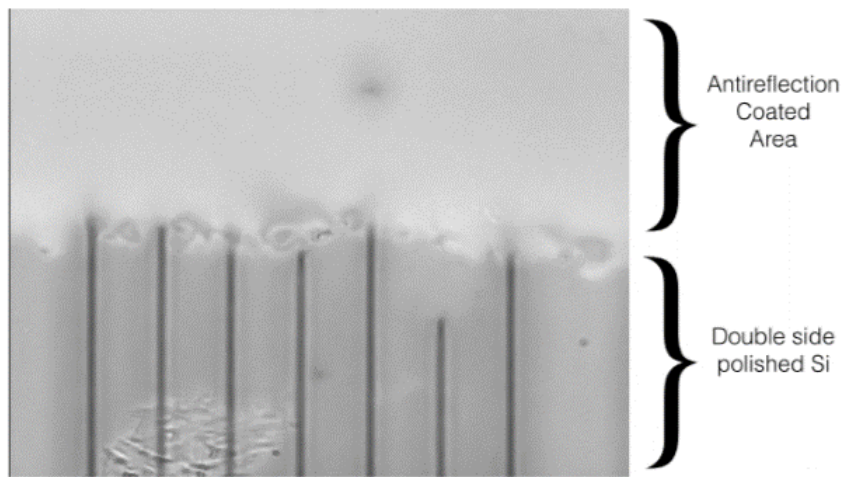
Figure 5.3: Microscope image of DSP-SSP boundary. In DSP region, modifications are formed. On the boundary, scribing is disrupted and no modification in SSP region.

Since the mechanism is not filamentation and the reflection has an effect in formation, we believe a temperature based mechanism, most likely thermal lensing might explain this phenomenon. High repetition rate of the laser provides a constant energy flow to the sample. In current configuration, each pulse arrives 6.7 μsec after the previous one. If the heat diffusion is slower than the crystal modification, flow of energy may continue in the laser propagation direction for long ranges, which results laser-writing in that direction. To test this idea, we increased the time difference between the pulses by decreasing the repetition rate

27

of the system while having the same pulse energy and peak power. We modified our MOPA system such that instead of pumping the amplifiers continuously and obtaining pulses with 150 kHz repetition rate, we used pulsed pump with the desired repetition rate. By arranging the duration of the amplifier pumps and the seed delay, we can adjust the pulse energy. Doing so, we were able to determine the impact of the heat accumulation on the mechanism. With this configuration, we decreased the repetition rate down to 2 kHz, which corresponds to 500 ms pulse-to-pulse time duration. We raster scanned the sample with this repetition rate and subsurface modifications were formed very uniformly. Since heat diffusion in silicon occurs in time scale of microseconds, this experiment rules out the thermal interaction between pulses as a factor in modification formation. However, thermal simulation of laser-silicon interaction is necessary to prove that phenomenon.

Our current theory on wall-like geometry of subsurface modifications suggests that forward propagating and reflected parts of the beam create heat reservoir for each other and interact nonlinearly. As a result, it causes beam to self-focus and modify silicon. We simulated the pulse propagation of a focused beam inside 500 μm thick bulk silicon with the existence of 200 μm long, 4 μm thick amorphous silicon. Our simulations showed that amorphous silicon inside bulk silicon can behave as a waveguide (Figure 5.4.a). Therefore, every pulse coming after, couples to modification created by the previous pulse and increases the length of the structure in laser propagation direction. Figure 5.4.b shows the illustration of the current theory.

Experiments and results given so far were crucial in understanding the possible mechanism. To elucidate the character of the creation of nano-walls deeply, we need further investigation of laser-material interaction parameters including polarization, doping concentration, incident power and scanning direction with respect to crystal orientation. Effects of change in these parameters are presented in the following subsections.
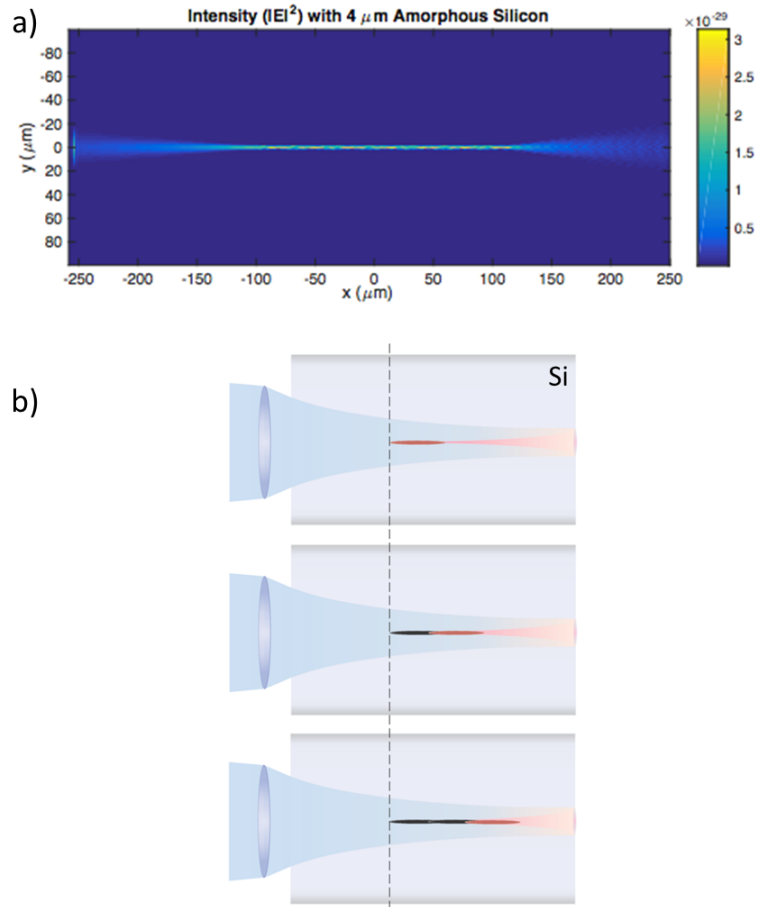
Figure 5.4: (a) Focused beam is guided by amorphous silicon buried inside crystal silicon. This can lead to high intensities outside the Rayleigh length. (b) Temporal evolution of the modifications. Uppermost subfigure shows the effect of the first pulse. Incident pulses extend the modifications in laser direction.

5.2 Laser and Sample Parameter Studies

5.2.1 Polarization

Polarization direction with respect to scanning direction may have significant effect on the modifications of materials. In several studies, it has been shown that different polarizations can change intensity of the modifications or they can effect plasma distribution [36, 37]. Moreover, it is also possible that polarization sensitivity of the processing can add another dimension to optical data storage

capabilities and increase the information density of the material [38]. Therefore, we decided to check the effect of polarization on our structures. For that purpose, as a first step, we studied linear polarization with vertical and horizontal scanning directions. As will be explained in Chapter 5.5, scanning direction doesn't alter the quality of the structures. Therefore, using a polarization with two different scanning axis can span all linear polarization interaction in xy plane. Thus, we raster-scanned the sample in direction parallel to horizontal polarization, then we switched the scanning direction to vertical and repeat the experiment. In these experiments, we kept the rest of the parameters unchanged, we used n-doped (1Ω.cm resistivity) samples and 22 μJ pulse energy. Figure 5.5.a and 5.5.b shows the results of horizontal and vertical scans respectively. From here it can be said that, linear polarization can be used with different scanning directions in processing without any distinguishable difference. However, a more detailed investigation is needed to support this observation. Although with microscope results, physical properties seem to be the same, their optical properties such as refractive index can be different.
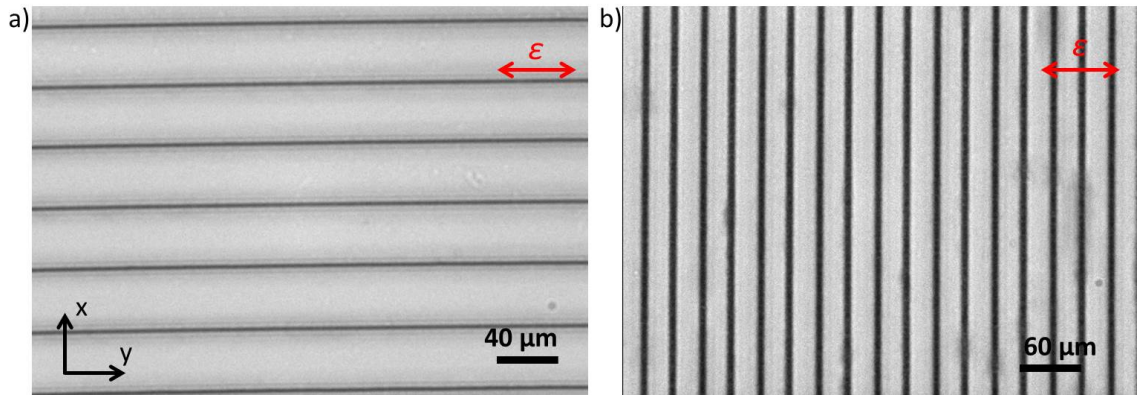
Figure 5.5: a) Microscope image of horizontal scanning with horizontal polarization (b)Microscope image of vertical scanning with horizontal polarization

Moreover, we created rectangular-mesh structures inside silicon. There are two reasons for this experiment. The first one is for further investigation of polarization-scanning direction relationship. To write these modifications, we used both horizontal and vertical polarizations and scanned in x and y directions for each of them (z-direction is laser propagation direction). By doing that, we

30

have a complete set of results that show effect of the polarization. The second reason is to see how previously written line interacts with the polarized laser by intersecting two perpendicular lines created with the same polarization. To do so, vertical lines are inscribed with vertical polarization and on the same processing area, again using vertical polarization, horizontal lines are inscribed. Further, complementary experiment is studied. We transformed the polarization to horizontal, and repeat the same processing procedure as with the vertical polarization. For the experiments, p-doped samples were used with pulse energy 22 μJ. Final structures in both experiments are in mesh pattern as desired. Results are presented in Figure 5.6.a and 5.6.b. It seems that in both cases, continuity is not disrupted by the existence of "wall" and no differences exist on the quality of the structures. For both polarizations, writing direction did not have any influence on the final structures.
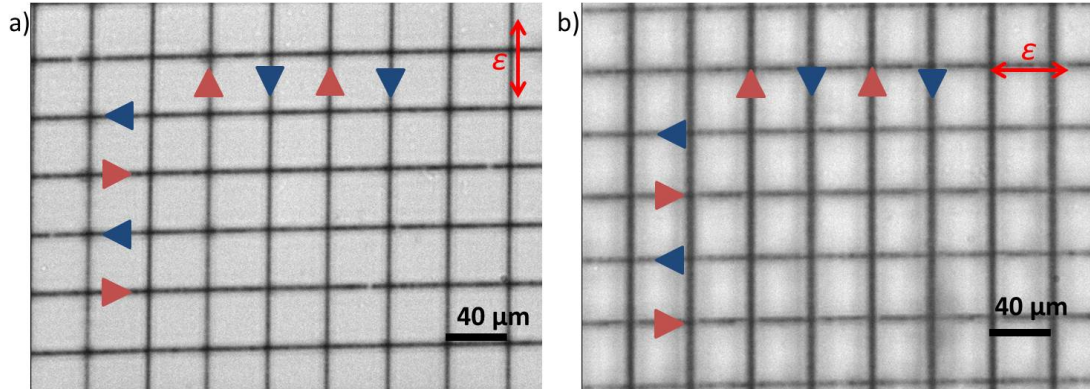
Figure 5.6: (a) Mesh pattern inscribed with vertical polarization. When the modifications intersect, there is no discontinuity and for both scanning direction, the quality is the same. (b) The same pattern with horizontal polarization. The quality is similar with the vertical polarization case.

5.2.2 Doping Concentration

As stated earlier, the aspect-ratio of the structures were quite high. A notable contrast between other 3D processing of transparent materials in the literature and our study is the type of the material. In previous studies, processed materials are generally dielectrics. The main difference of our work is that it is the first

time that bulk of a semiconductor is processed. That means contribution of free carriers can be important in silicon processing mechanism, whereas it can be neglected in the literature, since nonlinearity in silicon is directly effected by the interaction of electric field with electrons and phonons [39]. Therefore, we thought a feedback mechanism between photons and electrons can explain wall-like structures. If that is the case, then one may expect that the length of the structures must be different for different doping concentrations. To experiment this hypothesis, we selected three wafer types: undoped (Boron doped, 15 kΩ.cm), p-type (Boron doped, 1 Ω.cm) and n-type (Phosphorus doped, 1 Ω.cm). Each sample was raster-scanned in the vertical direction with horizontal polarization with the same incident power. Length obtained with SEM and length obtained with microscope data are shown in Table 5.1. Possible reason for n-doped silicon

Table 5.1: Doping concentration vs. Modification length

Doping Type	Length (SEM) (μm)	Length (Microscope) (μm)
p-type, 15 kΩ.cm	350	360
p-type, 1 Ω.cm	190	180
n-type, 1 Ω.cm	125	150

has the smallest size is that electron lifetime is smaller than hole lifetime [40]. As a result, photon-electron interaction takes less time,i.e., propagates smaller distance whereas photon-hole interaction takes longer distance before it lasts. However, regardless of doping type, a build up of electrons from free-carrier absorption together with thermal lensing can explain the formation of modifications.

5.2.3 Pulse Energy

The main mechanism of creating subsurface structures is nonlinear absorption. That indicates until a certain intensity, the light will pass through the material and above threshold nonlinear effects becomes dominant, starting the absorption. We determined the modification threshold for silicon empirically. When the refractive index change is large enough to create a visible intensity difference in

transmitted light, in other words, when the structures can be identified visually, threshold is reached. The lowest pulse energy to modify the bulk silicon is found to be 18.6 μJ, for all types of silicon we experimented. This result is surprising, because, as stated in Chapter 2, for optical breakdown a critical electron density must be reached. For n-doped silicon, the initial electron density will be much higher than the p-doped silicon, thus making it to require less pulse energy to reach the critical level. Considering this, one may expect threshold for n-type is lower than p-type.
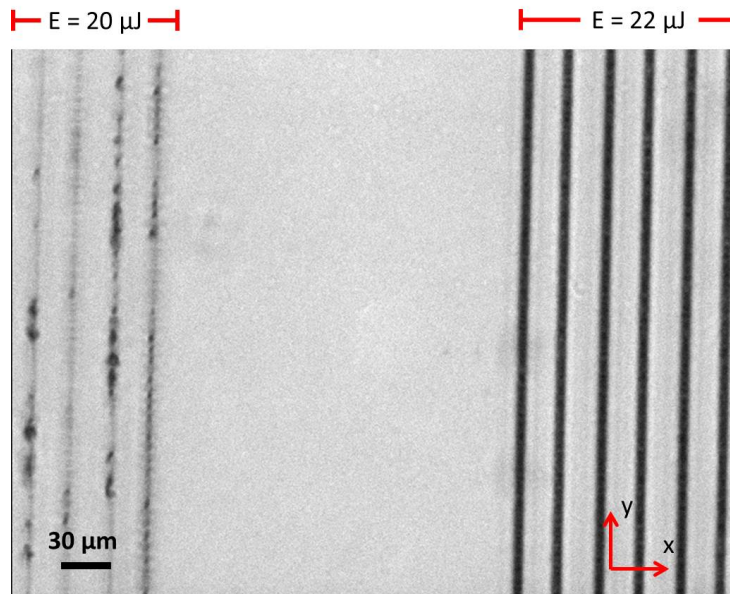
Figure 5.7: Comparison of the quality of the structures processed with 20 μJ and 22 μJ. Even though only energy levels are not the same, microscope images show that their refractive indexes are different as well.

Depending on the amount of excessive incident power above threshold, the quality of the modifications can vary dramatically. There are three regimes after threshold. In the first one, when the power is around lower limit, structures still occur, but their continuity are not at desired level and refractive index change is not very distinct. In extremely high-power regime, intensity on the surface is high enough for surface modification even though laser is focused deep in the silicon. Between these two levels, there is a limited regime where any power level can be chosen for continuous, high-quality processing. Experimentally, we found that

when we keep the pulse energy in the range of 19 μJ to 23.3 μJ, we obtain modifications without any discontinuity. Setting the power outside of this range results in either surface damage or weak structures. Such a change may be an indication of gradual refractive index change which requires further analysis. Corresponding intensities for these energy values are calculated as 1,58.10^{15} W/m^2 and 1,93.10^{15} W/m^2. Figure 5.7 shows the microscope images of two structures processed with 20 μJ and 22 μJ pulse energies on the same n-doped sample. 150 kHz repetition rate, 0.2 mm/sec scanning speed and 300 μm focus depth are kept the same for both structures. Structures on the right were inscribed with 22 μJ. Uniformity and continuity of the structures are superior to ones on the left.

In other experiment, on n-doped samples, we kept the scanning speed 0.2 mm/sec and focused the beam with NA = 1.3, X100 objective. We changed the pulse energy incrementally by rotating the half-wave plate in the power attenuator system. At low power levels no structure was observed. After the threshold level, they started to form discontinuously and at higher levels, they are fully continuous. The microscope image can be seen in Figure 5.8.
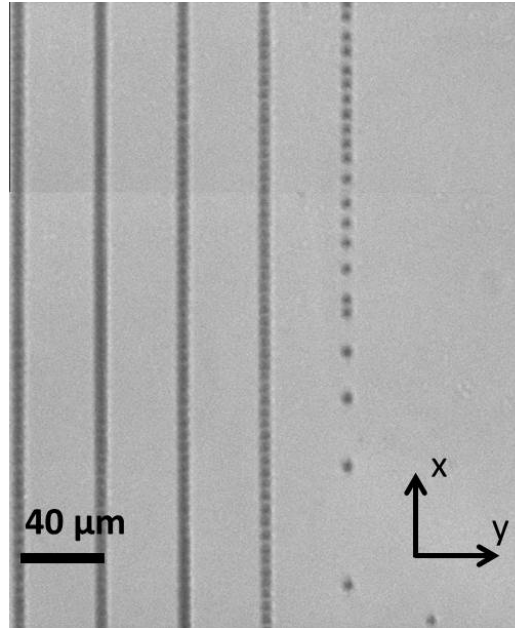

Figure 5.8: Result of gradual power increase. Incident power can determine the continuity of the structures by itself.

5.2.4 Scanning Direction

From the previous experiments, we know that as long as we are on crystal axis, or have a very small angle, structures seem to have similar properties. In order to understand if formation of structures depends on position with respect to crystal axis, we designed and conducted several experiments. First, in both n and p-type samples, we created lines with random angle with crystal axis. Further, to explore the capabilities of our method we inscribed several polygonal geometries such as squares and triangles. Moreover, to investigate if there is any critical angle that has effect on formation mechanism, we processed curved structures such as circle and spiral where angle between main axis and scanning direction changes from 0^0 to 90^0. Microscope images of those demonstrated structures can be seen in Figure 5.9. From that, it seems that even though angle between the scanning direction and the crystal angle has a non-zero value, structures are continuous. Therefore, it can be concluded that crystal orientation has no effect in mechanism.
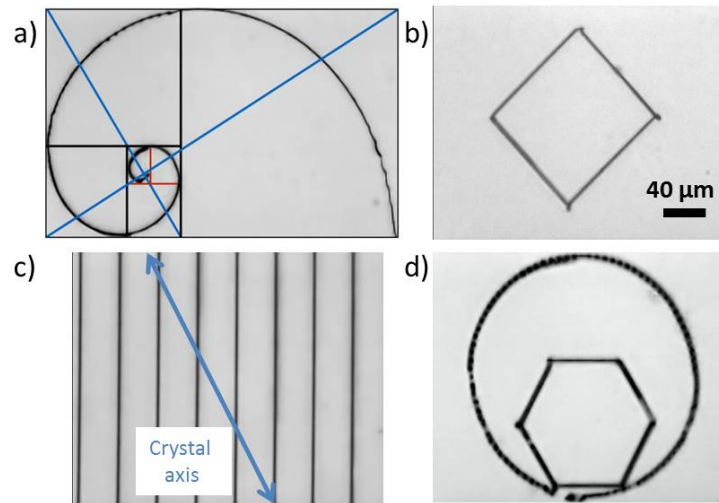

Figure 5.9: Different geometries can be processed with our method with axial freedom.

5.3 Applications

5.3.1 Multilayer Structures and Optical Data Storage

Large refractive index contrast created by processing can be utilized in design of photonic devices. One of these applications can be transformation of silicon into three-dimensional optical storage medium. Information can be recorded by focusing the laser and modifying the bulk of silicon. Similar approaches has been applied in a wide range of transparent materials [41, 42].

Critical parameters for high-density optical memory are the length of the modifications and precise control over the position of the structures. With the current configuration, the shortest obtainable structure length is around 200 μm. Given 500 μm thick wafer, it is possible to create two layers with different information encoding. However, it is inevitable to have some overlap between the structures with this length without damaging the surface. To overcome this problem and enrich the capability of the method, size of the structures should be decreased. Our understanding about the technique suggests that we need better focusing of the beam. Therefore, we used NA = 1.3, X100 objective to focus the beam in n-doped (1 Ω.cm) wafer for the experiment. The sample was raster scanned at the depth of 80 μm *(Level 1)*. Then, focus depth was increased to 120 μm and we repeated the procedure *(Level 2)*. The predicted positions are 276 μm and 414 μm for Level 1 and Level 2, respectively. Normally, to create structures at different levels, different power levels are required. However, for this experiment, the same pulse energy was enough for both levels. Figure 5.10 illustrates the fabrication procedure and SEM image corresponding to cross-section of Level 1 and Level 2 structures. From SEM image, it can be seen that structures are formed around calculated locations, which shows our control over the position of the modifications. Moreover, the size of the structures decreased below 100 μm.

Microscope images of two-level structures can be seen in Figure 5.11. When imaging plane is placed to Level 1, structures created at 80 μm depth are seen as thin, solid lines whereas Level 2 structures are as faint shadows. That is the case
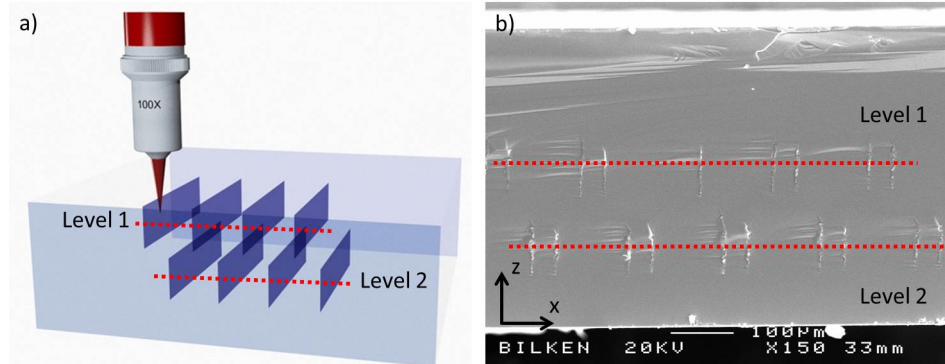
Figure 5.10: (a) Schematic of two-level structures. (b) SEM image of the structures. Positions for Level 1 and Level 2 are in good agreement with the calculations.

for Level 1 structures, when the imaging plane is shifted to 120 μm.
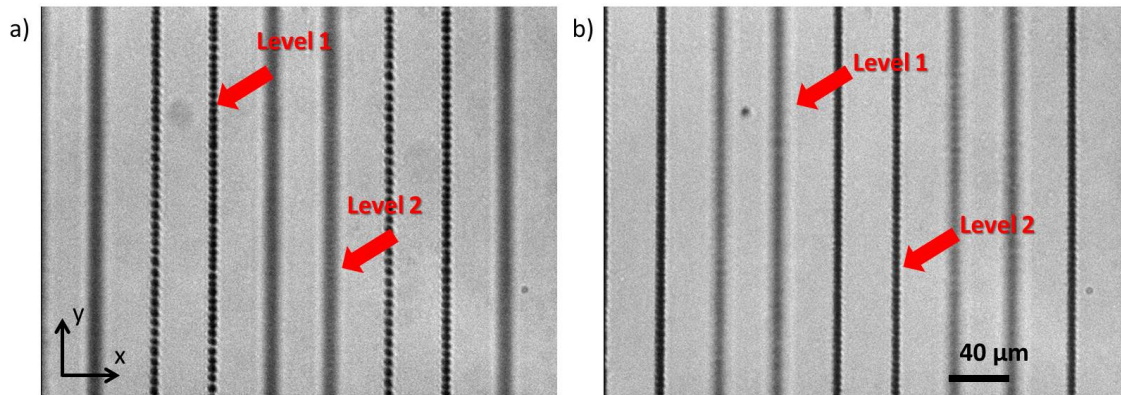
Figure 5.11: (a) Imaging plane is at Level 1. 2nd layer can be seen as faint shadow. (b) Image of the same xy plane when microscope objective is shifted to 120 μm in z-direction and focused on Level 2.

Using this ability, we demonstrated the utility of silicon as 3D optical data storage medium for the first time in literature. We created two barcode layers in n-doped silicon, with 22 μJ pulse energy and 0.2 mm/sec scanning speed. For focusing NA = 0.55 lens is deployed. Using Code-128 barcode symbology, we encoded "UFO" to level 1 and "LAB" to level 2. Thickness of the processed areas in barcodes is adjusted by writing the structures next to each other in a distance of 2 μm as much as needed. That close proximity of lines effectively provides a continuous processed range. Read-out of the information recorded in silicon was done with microscope. The same procedure used previously for reading two-level

37

structures was applied here as well. The only difference is that since two layers can not be imaged at the same frame, focus depth was kept fixed and imaging plane is moved on xy plane. Figure 5.12 shows the depth comparison of Level 1 and Level 2 barcodes.
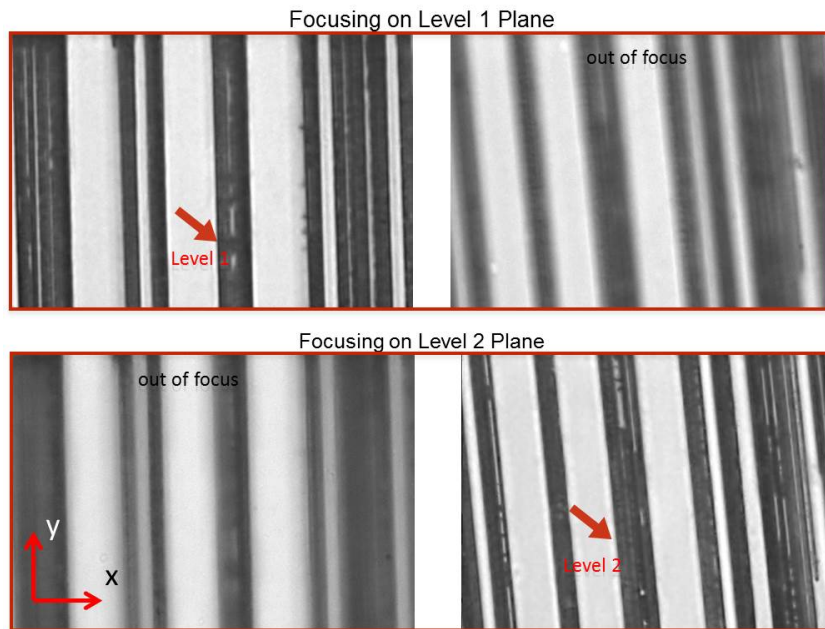

Figure 5.12: (a) Imaging plane is at Level 1. (b) Image of Level 2 structure when the objective is focused on Level 1. (c) The same xy plane on Level 1 structure as in (a) but imaging plane is at Level 2. (d) Focus of the microscope is on Level 2.

5.3.2   Fresnel Zone Plate

As another application, we fabricated the first functional optical device in bulk silicon. Refractive index contrast induced by processing can be utilized to build Fresnel zone plates buried in silicon. Fresnel zone plates are diffractive optical components, consist of concentric circles. Separation of the circles are adjusted such that light passing through the circles constructively interfere at some point [47]. Previously, surface zone plates on silicon has been studied [43] and it was fabricated by ion etching. So far, silica is the only material for direct laser writing of FZP in the bulk of a material [44, 45, 46].

Fabrication of phase-type zone plates can be achieved by creating concentric rings with alternating refractive indexes. For that purpose, we worked in focus after reflection regime, since modifications in this regime is more controllable, as explained in Chapter 5.1. In such configuration, focal length can be calculated by

$$R_n = \sqrt{nf\lambda} \tag{5.1}$$

where R_n is the radius of the outermost zone, n is the index of that zone, f is the focal length and λ is the wavelength of the light [47]. Using this equation, we designed a lens with outermost zone radius of 1.5 mm and has 20 zones. With a light source working at 1.5 μm, designed lens has a focal length of 25 cm in the silicon. Due to silicon-air interface, focal length gets shorter and using

$$f_{air} = \frac{f_{si}\lambda_{si}}{\lambda_{air}} \tag{5.2}$$

focal length in the air can be calculated as 7.24 cm. Assuming incident light is collimated, focused beam diameters is calculated as 46.09 μm. To fabricate this lens, we processed only even zones (n = 2, 4 ,6, ...20). Odd-numbered zones were left untouched as crystal silicon. In processed areas, we inscribed concentric circles such that each one is 10 μm wider than previously written circle. Scanning

speed of 0.2 mm/sec and 22 μJ pulse energy were used for structuring. Figure 5.13 shows written zone plate. Inset is the close-up of randomly selected area, that shows the overall quality. As a light source for the characterization of FZP,
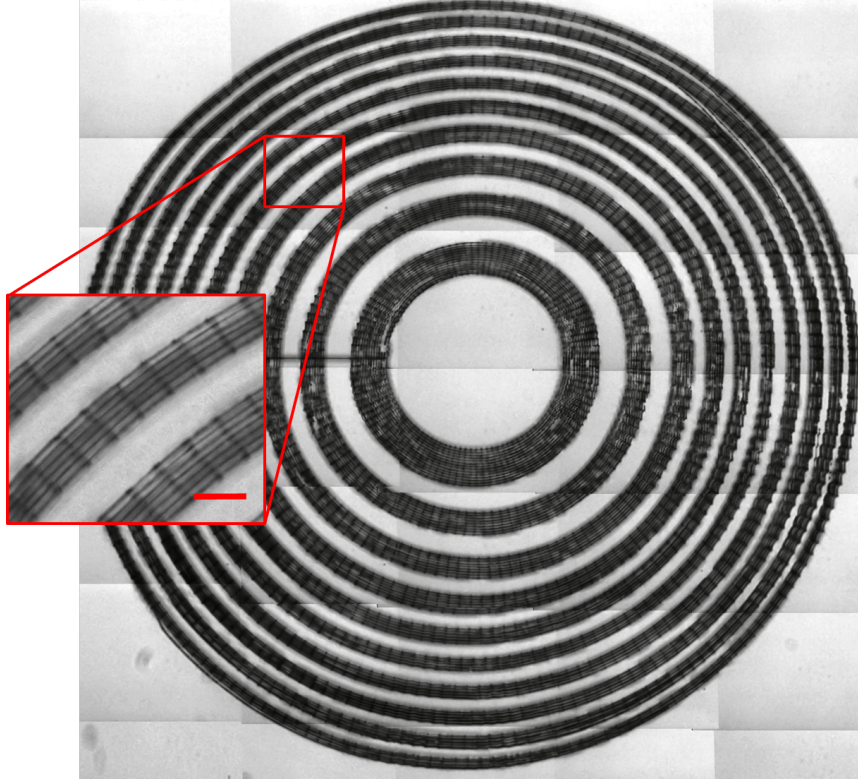
Figure 5.13: IR microscope image of Phase-type Fresnel zone plate. Dark zones corresponds to the laser-written areas. Scale bar indicates 70 μm.

since it works at 1.55 μm, we utilized our processing laser in low-power mode. Focusing properties of the lens was investigated with a beam profiler. Figure 5.14 shows the radius of the focused beam with respect to distance from the fabricated zone plate as well as the gaussian fitting with the same beam width. Beam quality of the output measured as $M^2 = 1.46$. Both axis has the same quality factor, which means FZP is circularly symmetric as expected. Focal length of the lens is approximately 7.5 cm, which is in good agreement with the calculations. However, at the focal point, spot size was measured as 128 μm. When it is compared with the theoretical result, divergence is not negligible. Moreover, diffraction efficiency was measured around 15 %. Although, maximum theoretical efficiency for phase-type zone plates is approximately 40 %, efficiency of our lens is comparable to the

most of the studies in the literature for one-layer of structuring. In silica glass, phase-type diffractive lenses typically have 17 % efficiency [48]. Precise control over the length of the structures can help for better design and higher efficiency.
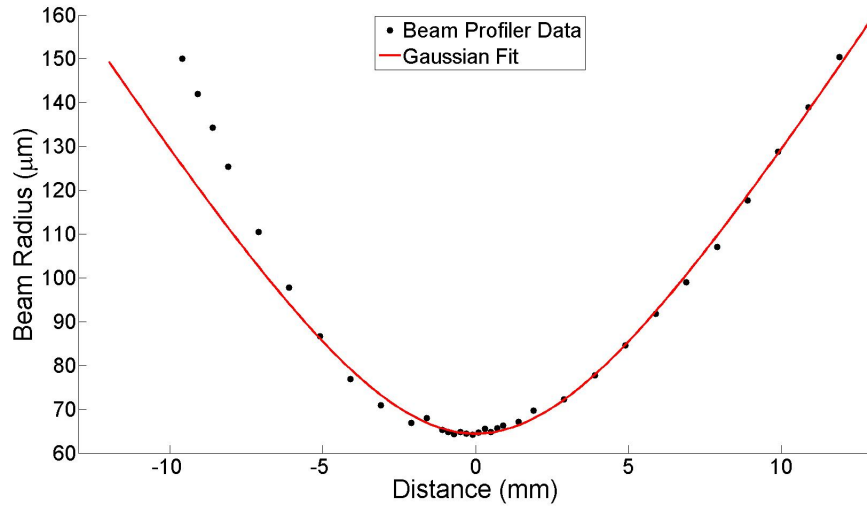
Figure 5.14: Focused beam diameter as a function of position. The beam profiler data (black) is fitted with a focused gaussian ($M^2 = 1.46$) shown with the curve in red.

Fabrication of an optical component buried deep in silicon demonstrate that silicon can be used for alignment-free, multi-lens systems working in mid-IR. Moreover, since Fresnel zone plates are diffractive component, it is possible to utilize silicon in holographic applications.

Chapter 6

Conclusion

In summary, we have shown the first subsurface modifications in silicon with a photo-induced, maskless process. This novel method allowed us to create higher refractive index in processed area than the rest of silicon in a controllable and predictable manner without damaging either front of back surfaces. Considering the wide studies in bulk processing of glass and other transparent materials for optical applications, we believe that we open a new field of research where bulk silicon will be studied to fabricate various optical devices.

For interior silicon processing, we have utilized a master-oscillator, power amplifier system working at 1.5 μm generating 5.5 ns pulses at 150 kHz repetition rate and producing 5 W average power. To reach the required intensities for inducing nonlinear absorption, create modifications with complex geometries and investigate the mechanism of the technique, we have designed and implemented a processing station that enable us to span a wide set of experimental parameters.

Four imaging methods have been developed for analysis and characterization of subsurface structures in silicon. These are infrared transmission microscopy, scanning electron microscopy, chemical etching and optical coherence tomography. All these methods were used to characterize the interior silicon for the first time in literature and give consistent results with each other.

Characterization of the modified structures revealed that length of the modifications in laser propagation direction is longer than Rayleigh length. Some of the possible reasons for these wall-like structures such as filamentation and heat accumulation have been eliminated. Currently, the most plausible explanation is the nonlinear interaction between the forward and reflected parts of the beam causes modifications and every other pulse extends the structures. Furthermore, effects of polarization, doping concentration, incident pulse energy, scanning direction on quality and continuity of the modifications have been studied.

After characterization of the subsurface modifications and mechanism studies, the next logical step is to utilize the knowledge we obtained to fabricate functional devices buried in silicon. By recording different information on different layers, we have employed silicon as an optical storage medium for the first time in literature. Moreover, we fabricated a Fresnel zone plate with high diffraction efficiency deep in silicon. In both applications, good agreement between the calculation and measurements shows our control and understanding over the process.

We believe that this new technique can be quite useful in fabrication of new devices in a wide range of area, including optoelectronics, silicon photonics and optofluidics. Therefore, new device designs in these areas using this method can be a target for future work. A more detailed investigation of optical and electrical properties of modification can be further studied. Numerical studies as well as effect of the pulse duration can be important milestones for understanding the mechanism fully.

Bibliography

[1] D. Liang, G. Roelkens, R. Baets, and J. E. Bowers, "Hybrid integrated platforms for silicon photonics," *Materials*, vol. 3, no. 3, pp. 1782–1802, 2010.

[2] E. Kuramochi, K. Nozaki, A. Shinya, K. Takeda, T. Sato, S. Matsuo, H. Taniyama, H. Sumikura, and M. Notomi, "Large-scale integration of wavelength-addressable all-optical memories on a photonic crystal chip," *Nature Photonics*, vol. 8, no. 6, p. 474—481, 2014.

[3] B. Jalali and S. Fathpour, "Silicon photonics," *Journal of Lightwave Technology*, vol. 24, no. 12, pp. 4600–4615, 2006.

[4] A. J. Pedraza, J. D. Fowlkes, and D. H. Lowndes, "Silicon microcolumn arrays grown by nanosecond pulsed-excimer laser irradiation," *Applied Physics Letters*, vol. 74, no. 16, pp. 2322–2324, 1999.

[5] G. D. Tsibidis, M. Barberoglou, P. A. Loukakos, E. Stratakis, and C. Fotakis, "Dynamics of ripple formation on silicon surfaces by ultrashort laser pulses in subablation conditions," *Physical Review B*, vol. 86, p. 115316, Sep 2012.

[6] M. Shen, J. E. Carey, C. H. Crouch, M. Kandyla, H. A. Stone, and E. Mazur, "High-density regular arrays of nanometer-scale rods formed on silicon surfaces via femtosecond laser irradiation in water," *Nano Letters*, vol. 8, no. 7, pp. 2087–2091, 2008.

[7] A. Serpengüzel, A. Kurt, I. İnanç, J. Carey, and E. Mazur, "Luminescence of black silicon," *Journal of Nanophotonics*, vol. 2, no. 1, pp. 021770–021770–9, 2008.

[8] A. Y. Vorobyev and C. Guo, "Laser turns silicon superwicking," *Optics Express*, vol. 18, pp. 6455–6460, Mar 2010.

[9] H. Misawa and S. Juodkazis, eds., *3D Laser Microfabrication.* Wiley-VCH Verlag GmbH & Co. KGaA, 2006.

[10] R. R. Gattass and E. Mazur, "Femtosecond laser micromachining in transparent materials," *Nature Photonics*, vol. 2, pp. 219–225, 2008.

[11] B. C. Stuart, M. D. Feit, S. Herman, A. M. Rubenchik, B. W. Shore, and M. D. Perry, "Nanosecond-to-femtosecond laser-induced breakdown in dielectrics," *Physical Review B*, vol. 53, pp. 1749–1761, 1996.

[12] C. W. Carr, H. B. Radousky, A. M. Rubenchik, M. D. Feit, and S. G. Demos, "Localized dynamics during laser-induced damage in optical materials," *Physical Review Letters*, vol. 92, pp. 87401–1——87401–4, Feb 2004.

[13] K. Davis, K. Miura, N. Sugimoto, and K. Hirao, "Writing waveguides in glass with a femtosecond laser," *Optics Letters*, vol. 21, pp. 1729–1731, 1996.

[14] Y. Nasu, M. Kohtoku, and Y. Hibino, "Low-loss waveguides written with a femtosecond laser for flexible interconnection in a planar light-wave circuit," *Optics Letters*, vol. 30, pp. 723–725, Apr 2005.

[15] A. Kowalevicz, V. Sharma, E. Ippen, J. Fujimoto, and K. Minoshima, "Three-dimensional photonic devices fabricated in glass by use of a femtosecond laser oscillator," *Optics Letters*, vol. 30, pp. 1060–1062, 2005.

[16] A. Crespi, Y. Gu, B. Ngamsom, H. J. W. M. Hoekstra, C. Dongre, M. Pollnau, R. Ramponi, H. H. van den Vlekkert, P. Watts, G. Cerullo, and R. Osellame, "Three-dimensional mach-zehnder interferometer in a microfluidic chip for spatially-resolved label-free detection," *Lab Chip*, vol. 10, pp. 1167–1173, 2010.

[17] A. Crespi, R. Ramponi, R. Osellame, L. Sansoni, I. Bongioanni, F. Sciarrino, G. Vallone, and P. Mataloni, "Integrated photonic quantum gates for polarization qubits," *Nature communications*, vol. 2, p. 566, 2011.

[18] G. D. Marshall, A. Politi, J. C. F. Matthews, P. Dekker, M. Ams, M. J. Withford, and J. L. O'Brien, "Laser written waveguide photonic quantum circuits," *Optics Express*, vol. 17, pp. 12546–12554, Jul 2009.

[19] C. Gunn, "Cmos photonics for high-speed interconnects," *Micro, IEEE*, vol. 26, no. 2, pp. 58–66, 2006.

[20] L. P. Carloni, P. Pande, and Y. Xie, "Networks-on-chip in emerging interconnect paradigms: Advantages and challenges," in *Proceedings of the 2009 3rd ACM/IEEE International Symposium on Networks-on-Chip*, pp. 93–102, IEEE Computer Society, 2009.

[21] L. Landau and L. E.M., *Electrodynamics of Continuous Media*. Oxford: pergamon Press, 1984.

[22] D. Arnold and E. Cartier, "Theory of laser induced free-electron heating and impact ionization in wide-band-gap solids.," *Physical Review B*, vol. 46, pp. 15102 – 15115, 1992.

[23] S. Akhmanov, V. Vyspoukh, and A. Chirkin, *Optics of Femtosecond Laser Pulses*. Moscow: Nauka, 1988.

[24] A. Couairon and A. Mysyrowicz, "Femtosecond filamentation in transparent media," *Physical Reports*, vol. 441, pp. 47–189, Mar. 2007.

[25] W. Spitzer and H. Y. Fan, "Infrared absorption in n-type silicon," *Physical Review Letters*, vol. 108, pp. 268 – 271, 1957.

[26] M. Dinu, F. Quochi, and H. Garcia, "Third-order nonlinearities in silicon at telecom wavelengths," *Applied Physics Letters*, vol. 82, pp. 2954 – 2956, 2003.

[27] R. W. Boyd, *Nonlinear Optics*. Orlando: Academic Press, second ed., 2003.

[28] I. Pavlov, E. Dulgergil, E. Ilbey, and F. O. Ilday, "Diffraction-Limited, 10-W, 5-ns, 100-kHz, all-fiber laser at 1.55 um," *Optics Letters*, vol. 39, no. 9, pp. 2695–2698, 2014.

[29] T. C. Chandler, "MEMC Etch—A Chromium Trioxide-Free Etchant for Delineating Dislocations and Slip in Silicon," *Journal of Electrochemical Society*, vol. 137, no. 3, p. 944, 1990.

[30] D. Huang, E. A. Swanson, C. P. Lin, J. S. Schuman, W. G. Stinson, W. Chang, M. R. Hee, T. Flotire, K. Gregory, C. A. Puliafito, and J. G. Fujimoto, "Optical Coherence," *Science*, vol. 254, pp. 1178–1180, 1991.

[31] E. McLeod and C. B. Arnold, "Subwavelength direct-write nanopatterning using optically trapped microspheres.," *Nature Nanotechnology*, vol. 3, pp. 413–7, July 2008.

[32] S. Nolte, M. Will, J. Burghoff, and A. Tuennermann, "Femtosecond waveguide writing: a new avenue to three-dimensional integrated optics," *Appl. Phys. A Mater. Sci. Process.*, vol. 77, pp. 109–111, June 2003.

[33] G. D. Marshall, M. Ams, and M. J. Withford, "Direct laser written waveguide-Bragg gratings in bulk fused silica.," *Optics Letters*, vol. 31, pp. 2690–1, Sept. 2006.

[34] T. Amemiya, A. Ishikawa, Y. Shoji, and P. Hai, "Three-dimensional nanostructuring in YIG ferrite with femtosecond laser," *Optics Letters*, vol. 39, no. 2, pp. 212–215, 2014.

[35] S. Nemoto, "Waist shift of a Gaussian beam by plane dielectric interfaces.," *Applied Optics*, vol. 27, pp. 1833–9, May 1988.

[36] L. Arissian, D. Mirell, J. Yeak, S. Rostami, and J. Diels, "Multiphoton Processes and Attosecond Physics," vol. 125, pp. 379–383, 2012.

[37] N. A. Panov, V. A. Makarov, V. Y. Fedorov, and O. G. Kosareva, "Filamentation of arbitrary polarized femtosecond laser pulses in case of high-order Kerr effect.," *Optics Letters*, vol. 38, pp. 537–9, Feb. 2013.

[38] P. Zijlstra, J. W. M. Chon, and M. Gu, "Five-dimensional optical recording mediated by surface plasmons in gold nanorods.," *Nature*, vol. 459, pp. 410–3, May 2009.

[39] J. Leuthold, C. Koos, and W. Freude, "Nonlinear silicon photonics," *Nature Photonics*, vol. 4, pp. 535–544, July 2010.

[40] M. Tyagi and R. Overstraeten, "Minority carrier recombination in heavily-doped silicon," *Solid-State Electronics*, vol. 26, p. 577, 1983.

[41] E. N. Glezer, M. Milosavljevic, L. Huang, R. J. Finlay, T.-H. Her, J. P. Callan, and E. Mazur, "Three-dimensional optical storage inside transparent materials," *Optics Letters*, vol. 21, p. 2023, Dec. 1996.

[42] D. Rentzepis, A. Parthenopoulos, and M. Peter, "Three-Dimensional Optical Storage Memory," *Science*, vol. 245, pp. 843–845, 1989.

[43] T. Grulois, G. Druart, N. Guérineau, A. Crastes, H. Sauer, and P. Chavel, "Extra-thin infrared camera for low-cost surveillance applications.," *Optics Letters*, vol. 39, pp. 3169–72, June 2014.

[44] E. Bricchi, J. D. Mills, P. G. Kazansky, B. G. Klappauf, and J. J. Baumberg, "Birefringent Fresnel zone plates in silica fabricated by femtosecond laser machining," *Optics Letters*, vol. 27, no. 24, pp. 2200–2202, 2002.

[45] W. Watanabe, D. Kuroda, K. Itoh, and J. Nishii, "Fabrication of Fresnel zone plate embedded in silica glass by femtosecond laser pulses," *Optics Express*, vol. 10, no. 19, pp. 279–284, 2002.

[46] P. Srisungsitthisunti, O. K. Ersoy, and X. Xu, "Volume Fresnel zone plates fabricated by femtosecond laser direct writing," *Applied Physics Letters*, vol. 90, no. 1, p. 011104, 2007.

[47] F. L. P. Pedrotti and L. S., *Introduction to Optics*. Englewood Clifffs, NJ: Princeton-Hall International, Inc., second ed.

[48] K. Yamada, W. Watanabe, Y. Li, K. Itoh, and J. Nishii, "Multilevel phase-type diffractive lenses in silica glass induced by filamentation of femtosecond laser pulses," *Optics Letters*, vol. 29, no. 16, p. 1846, 2004.